

# Simultaneous measurements of temperature and CO<sub>2</sub> concentration employing diode laser absorption near 2.0 μm

Tingdong Cai · Guangzhen Gao · Minrui Wang ·  
Guishi Wang · Ying Liu · Xiaoming Gao

Received: 1 May 2014 / Accepted: 13 January 2015 / Published online: 23 January 2015  
© Springer-Verlag Berlin Heidelberg 2015

**Abstract** Simultaneous measurements of gas temperature and CO<sub>2</sub> concentration in combustion gases using an extended-wavelength diode laser sensor at 2.0 μm are reported. A CO<sub>2</sub> transition pair located near 5,006.140 and 5,010.725 cm<sup>-1</sup> is selected based on existing line-selection criteria. The gas temperature and CO<sub>2</sub> concentration are inferred from the peak heights of the  $1f$ -normalized WMS- $2f$  signals. Some important factors (modulation depth, total pressure, and species concentration) influencing the performance of the sensor are discussed. Validation experiments performed in a heated static cell indicated that the sensor has accuracies of 1.21 and 2.98 % for temperature and CO<sub>2</sub> concentration measurement. The demonstration in combustion gases produced by a burner illustrates the potential of the  $1f$ -normalized WMS- $2f$  sensor for combustion diagnosis.

## 1 Introduction

In the development of modern propulsion and combustion systems, information of the temperature, density, pressure, mass flux, gas species concentration, and velocity during the combustion process is needed to facilitate design advancements, improve efficiency, and reduce pollutant emissions [1]. New diagnostic techniques that can provide

fast, sensitive, non-intrusive, and reliable measurements are hence required for in situ monitoring of multiple flow-field parameters during combustion. A remarkable optical spectroscopy technique, tunable diode laser (TDL) absorption spectroscopy (TDLAS), has been actively researched over the past two decades and has been used successfully in many fields, such as environmental monitoring [2, 3], industrial process control [4, 5], and biomedical sensing [6, 7]. The use of tunable diode lasers is attractive since they are compact, robust, and capable of fast tuning. TDLAS has also been used for combustion applications. Many sensors based on TDLAS have been used successfully to provide in situ, time-resolved, line-of-sight measurements of multiple flow-field parameters such as temperature, concentration, pressure, density, mass flux, and velocity in various combustion environments [8–12].

It is well known that carbon dioxide (CO<sub>2</sub>) is the most important greenhouse gas and its main anthropomorphic source is the combustion of hydrocarbon fuel. Because it is one of the primary combustion products of hydrocarbon-fueled systems and otherwise occurs at very low levels in the ambient atmosphere, CO<sub>2</sub> is an attractive target gas to monitor in hydrocarbon-fueled systems as its concentration can be directly interpreted as an indicator of combustion efficiency. Hence, detection of CO<sub>2</sub> is crucial to environmental and energy utilization. Likewise temperature, as a fundamental parameter of combustion systems, determines the overall thermal efficiency. Simultaneous measurements of CO<sub>2</sub> concentration and temperature thus hold high potential for combustion diagnosis and control.

CO<sub>2</sub> has a rich absorption spectrum throughout the infrared region as shown in Fig. 1, where the absorption line strengths of CO<sub>2</sub> are plotted as a function of wavelength from 1 to 3 μm at a temperature of 1,000 K. Limited by the available telecommunication diode lasers and

T. Cai (✉) · G. Gao · M. Wang · Y. Liu  
College of Physics and Electronic Engineering, Jiangsu Normal  
University, Xuzhou 221116, People's Republic of China  
e-mail: caitingdong@126.com

G. Wang · X. Gao  
Laboratory of Atmospheric Physico-Chemistry, Anhui  
Institute of Optics and Fine Mechanics, The Chinese Academy  
of Sciences, Hefei 230031, People's Republic of China

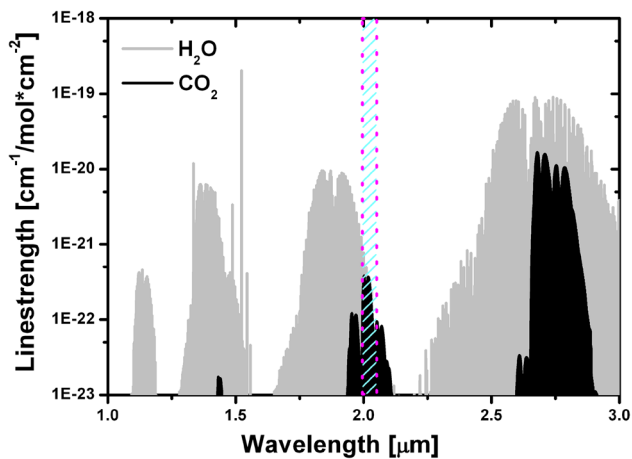


**Fig. 1** Absorption line strengths of CO<sub>2</sub> and H<sub>2</sub>O as a function of wavelength from 1 to 3 μm at a temperature of 1,000 K

optical fiber technology in the 1.3- to 1.6-μm-wavelength region, previous absorption sensors for CO<sub>2</sub> combustion diagnosis used the relatively weak combination bands near 1.55 μm ( $2\nu_1 + 2\nu_2 + \nu_3$ ) [13–15]. Measurements near 1.55 μm suffer from the small absorption transition strengths. This disadvantage led to sensing systems with relatively low signal-to-noise ratios and poor detection limits. With the availability of continuous-wavelength (cw) room-temperature single-mode diode lasers extending the spectral region to 3.5 μm [16], the  $\nu_1 + \nu_3$  and  $2\nu_2 + \nu_3$  bands near 2.7 μm have been used for monitoring CO<sub>2</sub> during combustion [17–20]. The CO<sub>2</sub> transitions in this region are approximately 1,000 times stronger than the transitions near 1.55 μm, and sensors based on these bands can therefore offer greater sensitivity and potential in their system measurements. Unfortunately, the CO<sub>2</sub> transitions in this region have substantial overlap with the strong transitions of H<sub>2</sub>O, which is the other primary combustion product of hydrocarbon fuel, as shown in Fig. 1. The CO<sub>2</sub> band near 2.0 μm ( $\nu_1 + 2\nu_2 + \nu_3$ ) can offer a 50 times improvement in absorption strength over the bands near 1.55 μm, is distant from the strong H<sub>2</sub>O absorption lines, and remains accessible within telecommunications-grade, fiber-coupled diode laser spectral ranges. Indeed, there are some studies of CO<sub>2</sub> combustion diagnosis using the transitions near 2.0 μm. For example, Webber et al. [21] developed an in situ CO<sub>2</sub> diagnostic for combustion applications that was based on a distributed-feedback diode laser operating at 1.997 μm. Mihalcea et al. [22] measured the concentration of CO<sub>2</sub> in high-temperature environments using an external cavity diode laser operating near 2.0 μm. Rieker et al. [23] measure the absorption spectra of the R46 through R54 transitions of the 20012 ← 00001 band of CO<sub>2</sub> near 2.0 μm ( $5,000 \text{ cm}^{-1}$ ) at pressures up to 10 atm. employing a TDL. However, all of these previous studies only measure

the concentration of CO<sub>2</sub> at high temperature or pressure rather than simultaneous measurements of temperature and CO<sub>2</sub> concentration using the transitions near 2.0 μm.

The work described herein introduces a sensor for the measurement of gas temperature and CO<sub>2</sub> concentration in a flame using diode lasers operating around 2.0 μm. To improve the detection sensitivity of the sensor and eliminate transmission variations of the laser due to beam steering, mechanical misalignments, soot, and window fouling,  $1f$ -normalized wavelength modulation spectroscopy (WMS) with second-harmonic detection, termed  $1f$ -WMS- $2f$ , is used in the measurement. The absorption transitions of CO<sub>2</sub> around 2.0 μm are analyzed to select the optimum line pair based on the HITRAN and HITEMP databases [24, 25]. A CO<sub>2</sub> line pair at 5,006.140 and 5,010.725  $\text{cm}^{-1}$  is selected for the TDL sensor using line-selection criteria established following design criteria previously reported in references [19] and [26]. The modulation depth for two different lasers used to access the selected CO<sub>2</sub> line pair is optimized to maximize the WMS- $2f$  signals and to simplify signal interpretation. The influence of variation of total pressure and CO<sub>2</sub> concentration during the measurement is also evaluated. First, the TDL sensor for gas temperature and CO<sub>2</sub> concentration measurement is validated in a heated cell containing well-controlled CO<sub>2</sub>-air mixtures. Then, measurements in a laboratory flame at atmospheric pressure are taken to demonstrate the potential of this sensor for use in combustion applications.

## 2 Theory

An accurate  $1f$ -normalized WMS- $2f$  model for absorption sensing at elevated temperatures was previously developed [5, 19, 26–29]. A brief review of the method is presented here to define the notation and guide the discussion.

For wavelength modulation spectroscopy, the laser is modulated by sinusoidally varying an injection current at angular frequency  $\omega = 2\pi f$  to produce laser frequency modulation (FM) and intensity modulation (IM):

$$\nu(t) = \bar{\nu} + a \cos(\omega t), \quad (1)$$

$$I_0(t) = \bar{I}_0 [1 + i_0 \cos(\omega t + \psi_1) + i_2 \cos(2\omega t + \psi_2)] \quad (2)$$

where  $\nu(t)$  is the instantaneous optical frequency,  $I_0(t)$  is the laser emission intensity, and  $\psi_1$  is the phase shift between the intensity and frequency modulation. The quantities  $\bar{\nu}$  and  $\bar{I}_0$  are the average optical frequency and intensity of the laser. The two modulation amplitudes  $a$  and  $i_0$  are the maximum small-amplitude excursions of  $\nu(t)$  and  $I_0(t)$  around  $\bar{\nu}$  and  $\bar{I}_0$ , respectively.  $i_2$  is the nonlinear IM amplitude with phase shift  $\psi_2$ .

When the laser beam travels through an absorbing medium with uniform distribution of temperature and concentration, the wavelength-dependent transmission  $\tau$  is described by the Beer–Lambert law:

$$\tau(\nu) = \left(\frac{I_t}{I_0}\right) = \exp\left[-Px_iL \sum_j S_j(T)\phi_j\right], \tag{3}$$

where  $I_t$  and  $I_0$  are the transmitted and incident laser intensities,  $P$  [atm.] is the total pressure,  $x_i$  is the mole fraction of the absorbing species  $i$ ,  $S_j$  [cm<sup>-2</sup> atm.<sup>-1</sup>] is the line strength of the transition  $j$ ,  $\phi_j$  [cm] is the line-shape function normalized such that  $\int \phi_j(\nu)d\nu \equiv 1$ , and  $T$  [K] is the gas temperature. For an isolated transition,  $\tau$  is a periodic even function in  $\omega t$  and can be expanded in a Fourier cosine series:

$$\tau[\bar{\nu} + a \cos(\omega t)] = \sum_{k=0}^{\infty} H_k(\bar{\nu}, a) \cos(k\omega t). \tag{4}$$

For weak transitions ( $Px_iL \sum_j S_j(T)\phi_j \leq 0.1$ ), the components  $H_k(\bar{\nu}, a)$  can be described as

$$H_k(\bar{\nu}, a) = -\frac{Px_iL}{(1 + \delta_{k0})\pi} \int_{-\pi}^{\pi} \sum_j S_j\phi_j(\bar{\nu} + a \cos \theta) \cos k\theta d\theta. \tag{5}$$

$H_k$  is directly proportional to the species concentration  $x_i$  and path length  $L$  when the line-shape functions do not vary over the range of conditions found in the applications [27]. Note that in addition to the absorption parameters,  $H_k$  also depends on the modulation depth  $a$ . This effect can be mitigated by choosing a proper modulation index  $m$ , which is defined as

$$m = \frac{a}{\Delta\nu/2}, \tag{6}$$

where  $\Delta\nu$  is the full width at half maximum (FWHM) of the absorption line shape. For second-harmonic signal, the peak value occurs at  $m \sim 2.2$ .

The harmonics at the modulation frequency of the transmitted laser intensity are extracted by lock-in amplifiers with a bandwidth determined by a low-pass filter. The magnitude of the absorption-based WMS-2f and 1f signal can be described by a commonly used simple model, while the modulation depth is small [27]:

$$S_{2f}(\bar{\nu}) = \frac{G\bar{I}_0}{2} \left| H_2 - \frac{i_0}{2}(H_1 + H_3) \right|, \tag{7}$$

$$S_{1f}(\bar{\nu}) = \frac{G\bar{I}_0}{2} \left| H_1 - i_0(H_0 + \frac{H_2}{2}) \right|, \tag{8}$$

where  $G$  is the optical–electrical gain of the detection system.

For an isolated transition acquired in an optically thin sample, it is well known that  $H_2$  is maximal when  $H_1$  and  $H_3$  are zero at the line center. Hence, near the line center, the dominant term of the WMS-2f signal is the second Fourier component  $H_2$ , and the dominant term of the WMS-1f signal is  $H_0$ , which is close to unity. Thus, the magnitude of the absorption-based WMS-2f signal,  $S_{2f}(\bar{\nu})$  and  $S_{1f}(\bar{\nu})$ , as can be measured by a lock-in amplifier, can be reduced as:

$$S_{2f}(\bar{\nu}) \approx \frac{G\bar{I}_0}{2} H_2(\bar{\nu}) = -\frac{G\bar{I}_0}{2} \frac{PS(T)x_iL}{\pi} \int_{-\pi}^{\pi} \phi(\bar{\nu} + a \cos \theta) \cos 2\theta d\theta, \tag{9}$$

$$S_{1f}(\bar{\nu}) \approx \frac{G\bar{I}_0 i_0}{2}, \tag{10}$$

where  $G$  is the optical–electrical gain of the detection system.

Because the second harmonics of the WMS-2f signal are proportional to the laser intensity and electro-optical gain, the WMS-1f signal can be used to normalize the second harmonics of the WMS signals:

$$C = \frac{S_{2f}}{S_{1f}} = \frac{1}{i_0} H_2(\bar{\nu}). \tag{11}$$

The 1f-normalized WMS-2f signal,  $C$ , is a only function of laser parameters ( $i_0, a$ ) and gas parameters ( $P, T, x_i$ ). Comparison should be made directly between the WMS-2f simulations and measurements, eliminating the need for scaling between the two, as the laser parameters can be determined before the measurements [27].

Gas temperature can be obtained from the ratio of 1f-normalized WMS-2f signals at two selected wavelengths

$$R = \frac{C_2}{C_1} = \frac{S_2(T) \int_{-\pi}^{+\pi} \phi(\bar{\nu}_2 + a \cos \theta) \cos 2\theta d\theta}{S_1(T) \int_{-\pi}^{+\pi} \phi(\bar{\nu}_1 + a \cos \theta) \cos 2\theta d\theta} = f(T), \tag{12}$$

which is closely related to the ratio of absorption line strengths. Hence, the gas temperature can be inferred by comparison of the measured ratio  $R$  with the simulation of the ratio as a function of temperature after the gas pressure is known. The species concentration can then be determined from either of the 1f-normalized WMS-2f signal magnitudes at the two selected transitions.

### 3 Sensor development

#### 3.1 Transition selection

Sensor performance can be greatly improved by selecting the optimum transition. The transition selection procedure

must consider the conditions where the sensor will be applied. These conditions may include the expected range of temperature, gas composition and pressure, path length. In this work, the sensor will be intended for demonstration in a heated static cell and on a burner that can produce a uniform flame with a diameter of 12 cm. The tuning temperature ranges are 500–1,000 and 850–1,350 K for the cell and burner, respectively, with pressures of ~1 atm. During the hydrocarbon fuel combustion, the CO<sub>2</sub> concentration ranges from 5 to 25 % depending on the C/H ratio of the fuel.

Based on the information above, absorption spectra simulated using the HITRAN and HITEMP databases near 2.0 μm are computed and used to select a proper line pair of CO<sub>2</sub>. As the transition selection criteria for absorption-based thermometry have been discussed previously [17, 19, 26], here, we succinctly discuss some rules that are used to choose the optimal CO<sub>2</sub> line pair for temperature and CO<sub>2</sub> concentration measurements in atmospheric experiments.

### 3.1.1 Line strength of the transitions

To ensure the sensor has a high sensitivity, each transition should have a large line strength. Meanwhile, the “weak transition” assumption associated with wavelength modulation measurements requires that the peak absorption should be less than ~0.1. The value at different conditions can be calculated using the needed parameters listed in the HITRAN and HITEMP databases.

### 3.1.2 Isolation from interference of other absorptions

The selected transitions must be free from interference by neighboring CO<sub>2</sub> and H<sub>2</sub>O transitions, so as to avoid inaccuracies in the measurement being introduced by the overlap of these different absorbances.

### 3.1.3 Relation between the ratio of WMS-2f signals and temperature

To obtain the gas temperature through the measurement of the ratio of WMS-2f signals, the relation between them must be monotonic over the measured range of temperatures. It can be seen from Eq. (5) that the ratio of WMS-2f signals is closely related to the ratio of the individual line strengths. This means that the line strength ratio also must be single valued with temperature over the expected range.

### 3.1.4 Sensitivity of the sensor

Here, the sensitivity is defined as the unit change in the normalized absorption strength ratio. The relation between

the ratio and the change in the normalized temperature can be described as

$$\left| \frac{\partial R/R}{\partial T/T} \right| = \left( \frac{hc}{k} \right) \frac{|E_1'' - E_2''|}{T}, \quad (13)$$

where  $E''$  is the lower state energy (cm<sup>-1</sup>) [5]. The relation indicates that a larger difference between the lower state energies yields an increase in sensitivity for the temperature measurement. For example, if the 2f peak heights can be determined within 1 %, to obtain a temperature accuracy of 3 % over the temperature range of 850–1,350 K, the constraint on minimum lower state energy difference could be given as follows, where the influence of line-shape function is neglected [28]:

$$\begin{aligned} |\Delta E^{\text{âL}^{\text{TMâL}^{\text{TM}}}}| &= |E_1^{\text{âL}^{\text{TMâL}^{\text{TM}}} - E_2^{\text{âL}^{\text{TMâL}^{\text{TM}}}}| \geq \left| \frac{dR_{2f}/R}{dT/T} \right| \times T \times \frac{k}{hc} \\ &= \frac{0.01\sqrt{2}}{0.03} \times 1,300 \times \frac{1}{1,4388} \approx 400 \text{ cm}^{-1}. \end{aligned} \quad (14)$$

### 3.1.5 Line-shape functions of the selected transitions

As shown in Eq. (5), the ratio of the WMS-2f signals peak height also depends on the pressure and species concentration as an effect of the line-shape function. This dependency complicates the measurement and introduces uncertainty. Fortunately, these effects can be overcome by choosing two transitions with similar air-broadened half-widths, self-broadened half-widths, and temperature-dependent coefficients, which are important factors for line-shape function.

Ultimately, based on the above criteria, the two transitions at 5,006.140 and 5,010.725 cm<sup>-1</sup> are chosen. Selected spectral parameters of the two transitions at different temperatures are listed in Table 1. Figure 2 shows the simulated CO<sub>2</sub> 2f signals for the selected line pair using these parameters for  $P = 1$  atm.,  $T = 1,000$  K,  $L = 10$  cm, and

**Table 1** Some spectral parameters of the two selected transitions at three different temperatures

$\nu$ (cm <sup>-1</sup> )	S (cm <sup>-2</sup> atm <sup>-1</sup> )	$\gamma_{\text{air}}$ (cm <sup>-1</sup> )	$\gamma_{\text{self}}$ (cm <sup>-1</sup> )	$E''$ (cm <sup>-1</sup> )	$n$
5,006.140					
@ 500 K	3.62E-3	0.0448	0.074	843.0300	0.76
@ 1,000 K	1.37E-3	0.0265	0.074	843.0300	0.76
@ 1,300 K	6.66E-4	0.0217	0.074	843.0300	0.76
5,010.725					
@ 500 K	1.15E-3	0.0472	0.067	1,333.7678	0.71
@ 1,000 K	8.65E-4	0.0288	0.067	1,333.7678	0.71
@ 1,300 K	4.94E-4	0.0239	0.067	1,333.7678	0.71

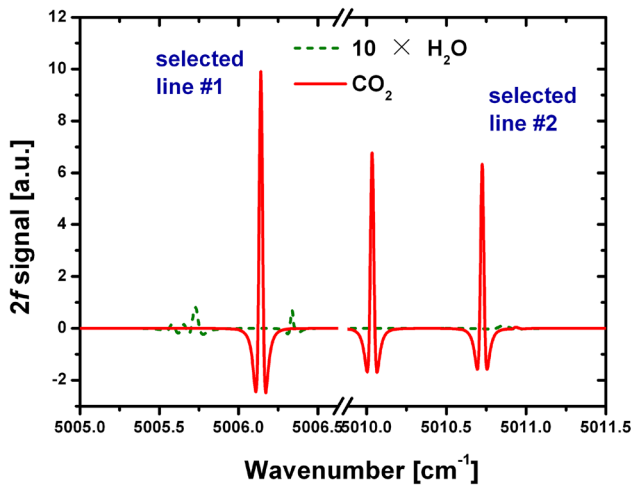


**Fig. 2** Simulated CO<sub>2</sub> 2*f* signals for the selected line pair for  $P = 1$  atm.,  $T = 1,000$  K,  $L = 10$  cm, 10 % CO<sub>2</sub>, 10 % H<sub>2</sub>O in air. The H<sub>2</sub>O signals are multiplied by a factor of 10 for clarity

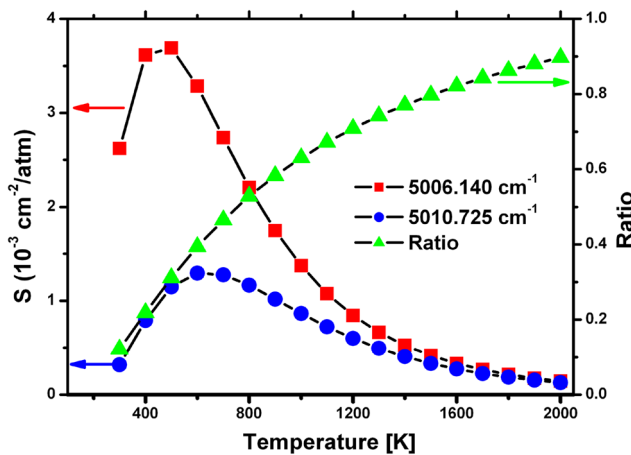


**Fig. 3** Line strength and their ratio of the selected transition pair as a function of temperature in the temperature range of 300–2,000 K

10 % CO<sub>2</sub>, 10 % H<sub>2</sub>O in air. The simulated H<sub>2</sub>O signals are multiplied by a factor of 10 for clarity. The line strength and their ratio of the transition pair are plotted in Fig. 3. All the figures and table help validate the selection of the transition pair.

### 3.2 Modulation depth optimization

It can be seen from Eq. (5) that the magnitudes of the WMS harmonic signals also depend on the modulation depth  $a$ . Because the FWHM  $\Delta\nu$  of the absorption line shape changes as the temperature varies, the modulation depth  $a$  under the proper modulation index  $m$  ( $\sim 2.2$ ) is also varied, as seen in Eq. (6). If the modulation depth  $a$  is set as  $1.1\Delta\nu$  at a certain temperature, the magnitude of the WMS-2*f*

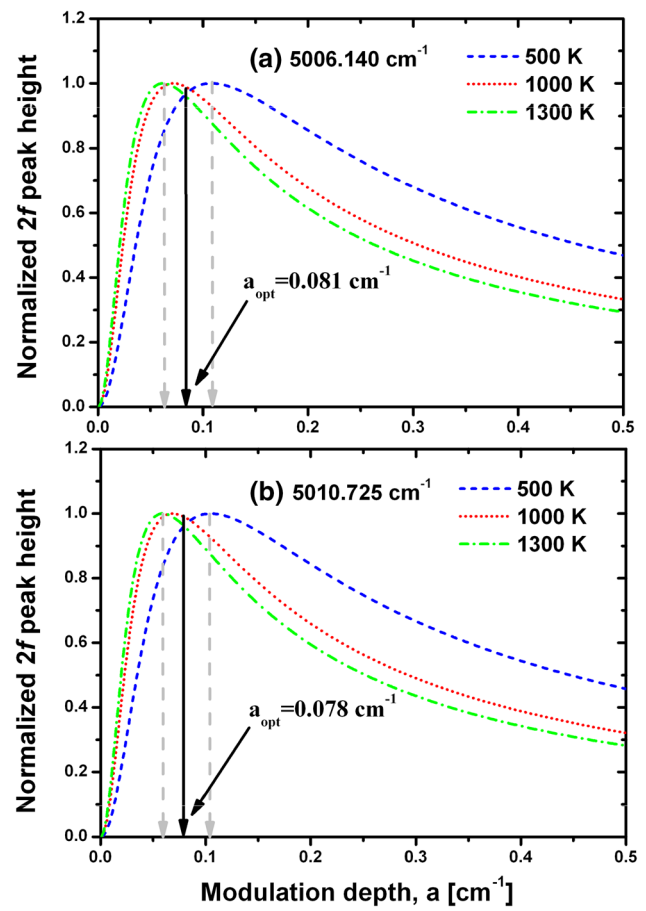


**Fig. 4** Simulated normalized WMS-2*f* peak heights versus modulation depth at three temperatures ( $T = 500, 1,000, 1,300$  K),  $P = 1$  atm., 10 % CO<sub>2</sub> in air, and path length  $L = 10$  cm. **a** and **b** are for the selected CO<sub>2</sub> transitions near 5,006.140 and 5,010.725 cm<sup>-1</sup>, respectively

signal cannot be kept at a maximum over the target temperature range. This will influence the sensor performance. To mitigate this influence, an optimal modulation depth can be selected for the two lasers used for the sensor. The optimal modulation depth can be defined as a value at which the peak height of the WMS-2*f* signal remains relatively strong over the expected temperature range. The best way for selecting the optimal modulation depth is to simulate the 1*f*-normalized WMS-2*f* signal at the target gas conditions as a function of modulation depth.

The simulated normalized WMS-2*f* peak heights are plotted in Fig. 4a, b for the selected CO<sub>2</sub> transitions near 5,006.140 and 5,010.725 cm<sup>-1</sup> versus modulation depth at three temperatures ( $T = 500, 1,000, 1,300$  K), with  $P = 1$  atm., 10 % CO<sub>2</sub> in air, and path length  $L = 10$  cm. The functionality is due entirely to integral in Eq. (9) for  $S_{2f}(\bar{\nu})$ . The simulation is based on a Voigt profile [30] with the spectral parameters listed in Table 1. As shown in Fig. 4a, the optimum modulation depth  $a$  decreases from  $\sim 0.11$  to  $\sim 0.07$  cm<sup>-1</sup> as temperature increases from 500

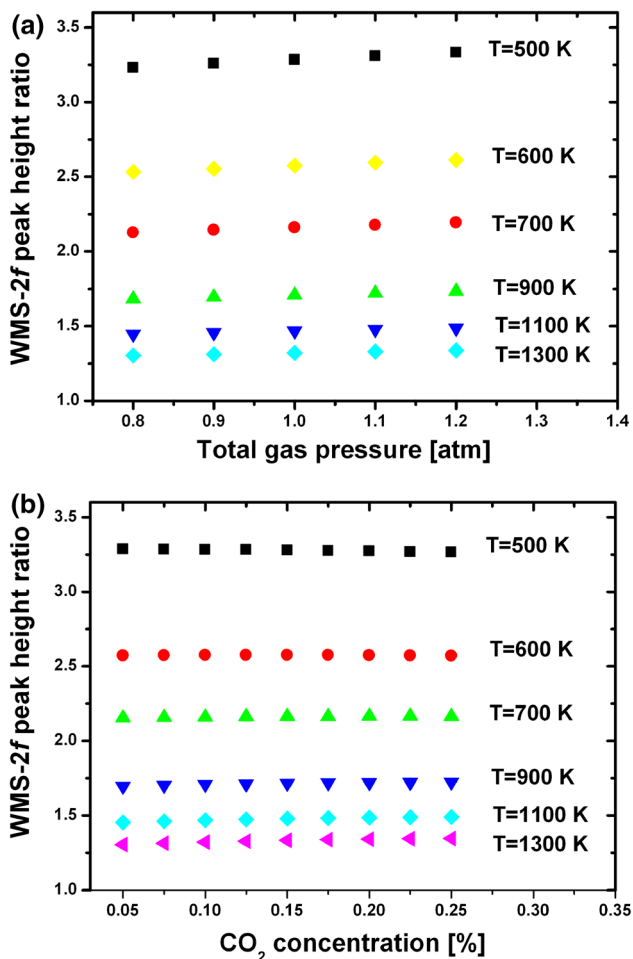


**Fig. 5** Simulated  $2f$  peak height ratios of the selected transition pair ( $5,006.140/5,010.725\text{ cm}^{-1}$ ) as a function of total pressure (**a**  $X_{\text{CO}_2} = 10\%$ ) and  $\text{CO}_2$  concentration (**b**  $P = 1\text{ atm.}$ ), respectively

to 1,300 K, reinforcing the statement that the optimum modulation depth  $a$  occurs where the modulation index  $m$  is around 2.2. Here, we selected  $a_{\text{opt}} = 0.081\text{ cm}^{-1}$  as the optimum modulation depth for the  $\text{CO}_2$  transition at  $5,006.140\text{ cm}^{-1}$  for all temperatures. With this optimum modulation depth, the WMS- $2f$  peak height has a fairly large value and varies slowly over the target temperature range of 500–1,300 K. In the same way, an optimal modulation depth  $a_{\text{opt}} = 0.078\text{ cm}^{-1}$  is selected for the other  $\text{CO}_2$  transition at  $5,010.725\text{ cm}^{-1}$  for the range of expected conditions. By optimizing the modulation depth, the peak heights ratio of the WMS- $2f$  signals will mainly depend on the line strengths of the selected  $\text{CO}_2$  transitions pair and the gas temperature can be inferred correctly. Here, the modulation depths are chosen for atmospheric measurement of temperature over a range of 850–1,350 K. Of course, the same procedure can also be used to optimize the modulation depth for conditions with different temperatures and pressures.

### 3.3 Evaluation of the influence of pressure and species concentration

Because the WMS- $2f$  peak heights ratio is also a function of pressure and gas composition through their effect on the line-shape function as shown in Eq. (5), we evaluate here the influence of pressure and species concentration on the temperature measurement. Figure 5a, b illustrates the simulated WMS- $2f$  peak heights ratio of the selected transition pair ( $5,006.140/5,010.725\text{ cm}^{-1}$ ) as a function of total gas pressure and  $\text{CO}_2$  concentration at six different temperatures with the selected optimal modulation depths. The relation of the WMS- $2f$  peak heights ratio and the total gas pressure is plotted for a 10 %  $\text{CO}_2$ -air mixture over the pressure range of 0.8–1.2 atm. in Fig. 5a. A 40 % change in the total gas pressure only introduces a maximum change of 1.23 % in the WMS- $2f$  peak heights ratio at the six selected temperatures. The relation of the WMS- $2f$  peak heights ratio and the  $\text{CO}_2$  concentration is plotted for  $P = 1\text{ atm.}$  for a  $\text{CO}_2$  concentration range of 5 to 25 % in Fig. 5b. It can be seen from the figure that a fivefold change in  $\text{CO}_2$  concentration only produces a maximum change of 1.07 % in the WMS- $2f$  peak heights ratio. These results indicate that the WMS- $2f$  peak heights ratio is a strong function of the ratio of line strengths and is only weakly related to total gas pressure and  $\text{CO}_2$  concentration. Hence, an accurate gas temperature can be inferred from a reliable  $1f$ -WMS- $2f$  peak heights ratio in combustion diagnosis.

## 4 Measurement validation in a static cell

To validate the TDL sensor, the measurements of gas temperature and  $\text{CO}_2$  concentration are first taken in a heated static cell before being used in combustion applications. The static cell can provide a quiet, transient-free environment with well-controlled pressure, species concentration, and gas temperature. Thus, the measurement in a static cell is a useful way to confirm the accuracy and reliability of the sensor.

### 4.1 Experimental setup

The experimental arrangement used for the simultaneous measurement of gas temperature and  $\text{CO}_2$  concentration in a heated static cell is illustrated in Fig. 6. The heated static cell is made of stainless steel with a length of 30 cm and an inner diameter of 1.5 cm. Two sapphire windows with 1-cm open aperture are tapered in both ends to ensure the transmission of the light at  $2\text{ }\mu\text{m}$ . The surfaces of the window through which the beam passes have a  $1.2^\circ$  wedge to avoid residual etalon fringes. The temperature of the static cell is controlled by a temperature controller (type SKW)

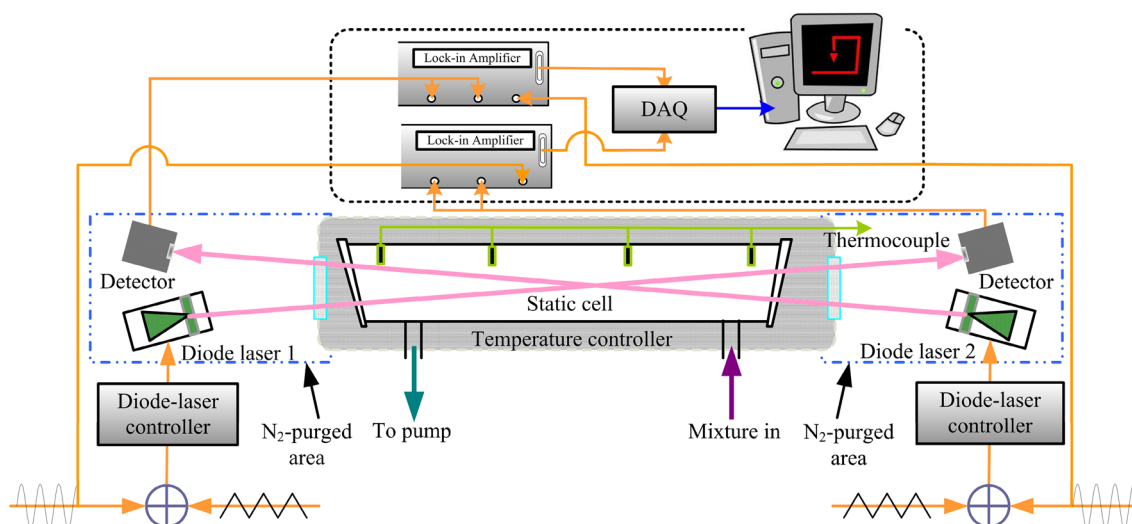


**Fig. 6** Scheme of the experimental setup

which can supply a temperature as high as 1,000 K. Four K-type thermocouples with accuracies of  $\pm 1\%$  and precision of 0.1 K are equally spaced within and attached to the absorption cell to monitor the temperature of the gas in the static cell. In the experiment, the permitted maximum temperature difference along the path length is no more than 5 K. The tested CO<sub>2</sub>–air mixtures are prepared using CO<sub>2</sub> gas with 99.99 % purity, mixed with ambient outdoor air in a stainless steel tank, and delivered into the cell via copper tubing. The  $\sim 390$ -ppm CO<sub>2</sub> contained in the air is considered in the preparation of the mixtures. A vacuum system is connected with the cell and the stainless steel tank via a stainless steel manifold. Pressure is determined with a vacuum pressure gauge with an accuracy of  $\pm 1\%$  of reading. Before each measurement, the gas sample was allowed to thermally stabilize.

Two identical commercial cw, thermoelectrically cooled, extended-wavelength distributed-feedback (DFB) tunable diode lasers operating near 2  $\mu\text{m}$  are used in the experiment. The laser power is about 2 mW, and the typical linewidth is  $\sim 2$  MHz. Frequency turning of the diode laser can be controlled by scanning either the temperature ( $\sim 0.63 \text{ cm}^{-1}/^\circ\text{C}$ ) or the current ( $\sim 0.03 \text{ cm}^{-1}/\text{mA}$ ). Here, the two lasers used for the absorption measurement at 5,006.14 and 5,010.725  $\text{cm}^{-1}$  are referred to as laser 1 and laser 2, respectively. The two DFB lasers are placed in commercial laser mounts (ILX Lightwave LDM-4980) and driven with modular diode laser controllers (ILX Lightwave LDC-3724). The wavelengths of the lasers are monitored by a free-space mid-IR wavelength meter (Bristol 621). To perform spectrometric measurements, the wavelengths of the DFB diode lasers are driven by a 0.7-kHz triangle ramp summed in an adder with a 49-kHz sine wave to provide the

wavelength modulation. After collimation, the TDL beams are collimated by lenses and sent through the static cell. The transmitted laser beams exiting the heated cell are focused onto two identical room-temperature extended-InGaAs detectors (Thorlabs, PDA10DT-EC). The beam paths are purged by high-purity nitrogen so as to avoid interference from ambient CO<sub>2</sub>. The detector signals are sent into digital lock-in amplifiers to demodulate the needed  $2f$  and  $1f$  data with the same time constant of 10  $\mu\text{s}$  for each laser. Both signals are sampled by a multifunction data acquisition (DAQ) card (ADLINK DAQ2010) in a desktop PC. A LabView program is used for data acquisition and analysis. Once the acquisition is completed, the signal-processing program transfers the captured data from on-board memory to the PC. Data analysis, including peak finding and ratio calculation, is then performed on the accumulated data.

## 4.2 Results

A set of static heated cell experiments with well-controlled CO<sub>2</sub>–air mixtures and temperatures is performed to confirm the sensor accuracy and reliability for the temperature and CO<sub>2</sub> concentration inferred from the  $1f$ -normalized WMS- $2f$  signals. All static heated cell experiments are performed at atmospheric pressure and in the temperature range of 500–1,000 K with a step of 50 K. Figure 7 shows the representative  $1f$  and  $2f$  signals obtained at 1,000 K with  $\sim 6.3\%$  CO<sub>2</sub> in air for the selected line pair. By normalizing the  $2f$  signal with the  $1f$  signal magnitude, common terms such as laser intensity, lock-in gain, laser transmission variation, and signal amplification can be eliminated.

The top graph in Fig. 8 is a comparison between the temperatures from the  $1f$ -normalized WMS- $2f$  sensor

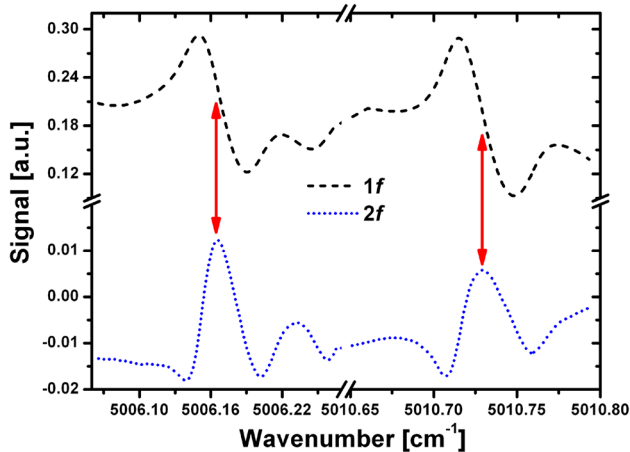


**Fig. 7** Representative  $1f$  and  $2f$  signals obtained in the static cell at 1,000 K with  $\sim 6.3\%$   $\text{CO}_2$  in air for the selected line pair

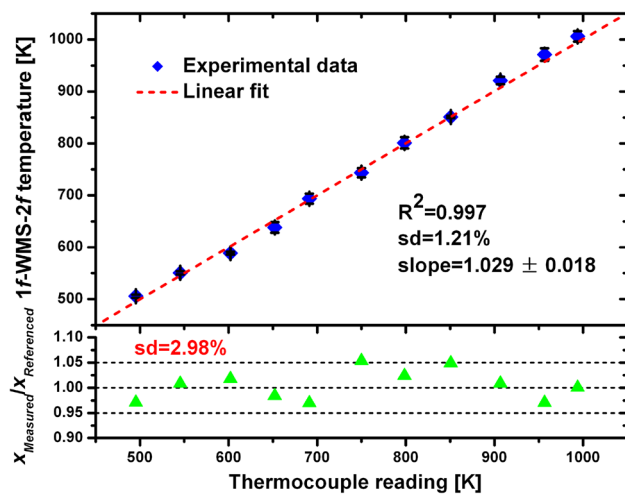


**Fig. 8** Comparison between the temperatures from the  $1f$ -normalized WMS- $2f$  sensor thermometry and the averages of the four thermocouple readings (*top graph*); ratio of the  $\text{CO}_2$  concentrations measured by the TDL sensor ( $x_{\text{Measured}}$ ) and the concentrations recorded when the mixtures were prepared ( $x_{\text{Referenced}}$ ) (*bottom graph*)

thermometry and the averages of the four thermocouple readings. The temperatures determined from the TDL sensor agree well with the thermocouple readings in the tested temperature range of 500–1,000 K. Correlation of those measured points has a square of the correlation coefficient  $R^2 = 0.997$ , and the average standard deviation is 1.21 %. The error bars are also shown in the graph. The linear-fitted slope is  $1.029 \pm 0.018$ , and the average bias between the measured values and the readings ( $\sigma_T = |P_{\text{TDL}} - P_{\text{TCR}}|$ ) is  $\sim 9$  K.

The bottom panel of Fig. 8 shows the ratio of the  $\text{CO}_2$  concentrations measured by the TDL sensor ( $x_{\text{Measured}}$ ) and the concentrations recorded when the mixtures were

prepared ( $x_{\text{Referenced}}$ ). The  $\text{CO}_2$  concentrations are measured using the  $\text{CO}_2$  transition at  $5,006.140 \text{ cm}^{-1}$  due to its stronger line strength over the other selected transition. Three measurements are taken for the  $\text{CO}_2$ -air mixture at each set temperature. The  $x_{\text{Measured}}$  is inferred from the average of the three measurements. The standard deviation between the measured and reference values is 2.98 % for the measurements of  $\text{CO}_2$  concentrations.

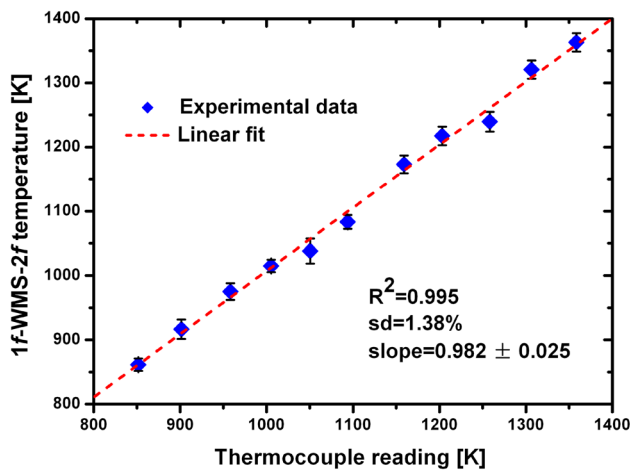
Errors in the temperature and concentration measurements primarily arise from uncertainties in the temperatures measured by the thermocouple, analysis of the measured spectroscopic data, and the referenced  $\text{CO}_2$  concentrations recorded during the preparation of the mixtures (especially for the low concentrations). The excellent agreement between the measured and reference values confirms the accuracy of the TDL sensor for the measurement of temperature and  $\text{CO}_2$  concentration employing the peak heights of the  $1f$ -normalized WMS- $2f$  signals.

## 5 Demonstration on a burner

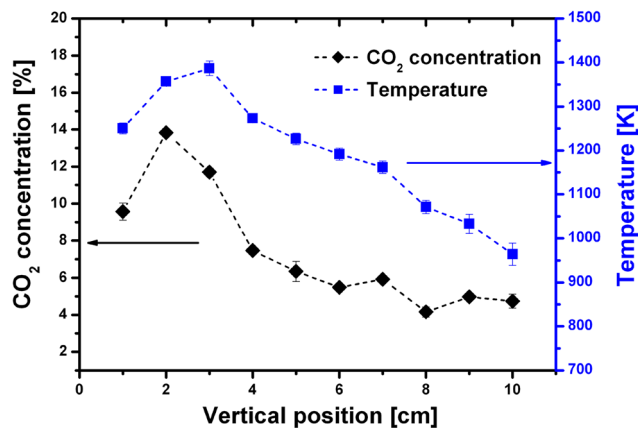
Measurements are also taken on a burner to illustrate the potential of the  $1f$ -normalized WMS- $2f$  sensor for monitoring the gas temperature and  $\text{CO}_2$  concentration in combustion gases. A burner that can produce an array of short diffusion flames served as the combustion test facility. The uniform flame on the burner has a circular shape with a diameter of 12 cm and a height of 2 cm. The  $2.0\text{-}\mu\text{m}$  extended-wavelength TDL sensor is driven by an external modulator, which consists of a 0.7-kHz triangle ramp combined with a faster 49-kHz sinusoidal signal. The two laser beams pass through the flame along its radial direction to probe the burned gases 1 cm above the burner. To avoid interference from ambient  $\text{CO}_2$ , the beam paths are also purged by high-purity nitrogen. The  $1f$  and  $2f$  components of the transmitted laser signals are obtained by digital lock-in amplifiers with the same time constant of  $10 \mu\text{s}$ . During the measurement, a thermocouple is traversed forward and back to confirm stability of the flame temperature using a sliding guide. The readings of the thermocouple are also used to compare with the temperature obtained by the TDL sensor. The combustion flow field studied here should be sufficient to assume as an approximate uniform temperature distribution in reducing the data.

Figure 9 shows the comparison between the temperatures from the TDL sensor and the thermocouple readings measured in the combustion gases. They are also in good agreement over the tuning temperature range of 850–1,350 K. Correlation of those measured points has a square of the correlation coefficient  $R^2 = 0.995$ , and the average standard deviation is 1.38 %. Error bars are also shown in the graph. The linear-fitted slope is  $0.982 \pm 0.025$ , and the





**Fig. 9** Comparison between the temperatures from the TDL sensor and the thermocouple readings measured in the combustion gases



**Fig. 10** Distributions of the gas temperatures and CO<sub>2</sub> concentrations as a function of vertical position in the combustion gases

average bias between the measured values and the readings ( $\sigma_T = |P_{\text{TDL}} - P_{\text{TCR}}|$ ) is  $\sim 13$  K.

Vertical distributions of the gas temperatures and CO<sub>2</sub> concentrations are also measured on the burner. In this distribution measurement, the combustion temperature is set at  $\sim 1,350$  K by adjusting the fuel/air ratio. Measurements are taken across the burner along the radial direction at ten vertical locations with a step length of 1 cm. The distributions of the gas temperatures and CO<sub>2</sub> concentrations as a function of vertical position are shown in Fig. 10. It can be seen from the figure that there are large spatial variations for the gas temperature and CO<sub>2</sub> concentration along the vertical locations. The maximum values of the temperature and CO<sub>2</sub> concentration are in the flame envelope. As the measurement position is gradually moved away from the burner, the temperature and CO<sub>2</sub> concentration decrease dramatically owing to the

diffusion of heat and combustion products. It is coincident with the combustion phenomena.

## 6 Summary

In this work, simultaneous measurements of the gas temperature and CO<sub>2</sub> concentration are demonstrated by means of an extended-wavelength diode laser sensor at  $2.0 \mu\text{m}$ . The sensor is based on two CO<sub>2</sub> transitions near  $5,006.140$  and  $5,010.725 \text{ cm}^{-1}$ , which are chosen as the optimum line pair for the target temperature of  $500\text{--}1,350$  K at atmospheric pressure using previously defined selection criteria. The temperature and CO<sub>2</sub> concentration are determined by the peak heights of the  $1f$ -normalized WMS- $2f$  signals. In this way, influences of variation in laser intensity and electro-optical gain can be removed. To enhance the performance of the sensor, the influence of modulation depth, total pressure, and species concentration are also evaluated. Measurements are first taken for a quiet, transient-free environment produced by a heated static cell. The comparison between the measured values and the well-controlled gas temperature and CO<sub>2</sub> concentration confirm the accuracy and reliability of the sensor. The sensor is then applied to short diffusion flames on a burner to illustrate the potential of the  $1f$ -normalized WMS- $2f$  sensor for combustion diagnosis. In contrast to the earlier related research here are reported the first simultaneous measurements of gas temperature and CO<sub>2</sub> concentration in combustion gas by the CO<sub>2</sub> transitions at  $2.0 \mu\text{m}$ .

**Acknowledgments** The work is funded by the National Natural Science Foundation of China (No. 11104237, No. 61475068), the Open Research Fund of Key Laboratory of Atmospheric Composition and Optical Radiation, Chinese Academy of Sciences (No. 2012JJ04), and the Priority Academic Program Development of Jiangsu Higher Education Institutions (PAPD). We thank in particular Prof. Jow-Tsong Shy for the participation.

## References

1. C.F. Edwards, K.-Y. Teh, S.L. Miller. Development of low-energy-loss, high-efficiency chemical engines. Global Climate and Energy Project Technical Report (Stanford University, 2006)
2. J.P. Besson, S. Schilt, E. Rochat, L. Thévenaz, Ammonia trace measurements at ppb level based on near-IR photoacoustic spectroscopy. *Appl. Phys. B* **85**, 323–328 (2006)
3. L. Joly, B. Parvitte, V. Zeninari, G. Durry, Development of a compact CO<sub>2</sub> sensor open to the atmosphere and based on near-infrared laser technology at  $2.68 \mu\text{m}$ . *Appl. Phys. B* **86**, 743–748 (2007)
4. I. Linnerud, P. Kaspersen, T. Jaeger, Gas monitoring in the process industry using diode laser spectroscopy. *Appl. Phys. B* **67**, 297–305 (1998)
5. X. Liu, J.B. Jeffries, R.K. Hanson, K.M. Hinckley, M.A. Woodmansee, Development of a tunable diode laser sensor for

- measurements of gas turbine exhaust temperature. *Appl. Phys. B* **82**, 469–478 (2006)
6. S. Kanoh, H. Kobayashi, K. Motoyoshi, Exhaled ethane: an in vivo biomarker of lipid peroxidation in interstitial lung diseases. *Chest* **128**, 2387–2392 (2005)
  7. M.R. McCurdy, Y. Bakhrkin, G. Wysocki, R. Lewicki, F.K. Tittel, Recent advances of laser-spectroscopy based techniques for applications in breath analysis. *J. Breath Res.* **1**, 014001 (2007)
  8. D. Richter, D.G. Lancaster, F.K. Tittle, Development of an automated diode-laser-based multicomponent gas sensor. *Appl. Opt.* **39**, 4444–4450 (2000)
  9. J.A. Silver, D.J. Kane, P.S. Greenberg, Quantitative species measurements in microgravity flames with near-IR diode lasers. *Appl. Opt.* **34**, 2787–2801 (1995)
  10. B.T. Fisher, A.R. Awtry, R.S. Sheinson, J.W. Fleming, Flow behavior impact on the suppression effectiveness of sub-10-lm water drops in propane/air co-flow non-premixed flames. *Proc. Combust. Inst.* **31**, 2731–2739 (2007)
  11. M.G. Allen, Diode laser absorption sensors for gas-dynamic and combustion flows. *Meas. Sci. Technol.* **9**, 545–562 (1998)
  12. S.T. Sanders, J.A. Baldwin, T.P. Jenkins, D.S. Baer, R.K. Hanson, Diode-laser sensor for monitoring multiple combustion parameters in pulse detonation engines. *Proc. Combust. Inst.* **28**, 587–594 (2000)
  13. D.M. Sonnenfroh, M.G. Allen, Observation of CO and CO<sub>2</sub> absorption near 1.57  $\mu\text{m}$  with an external-cavity diode laser. *Appl. Opt.* **36**, 3298–3300 (1997)
  14. R.M. Mihalcea, D.S. Baer, R.K. Hanson, Diode-laser sensor for measurements of CO, CO<sub>2</sub>, and CH<sub>4</sub> in combustion flows. *Appl. Opt.* **36**, 8745–8752 (1997)
  15. R.M. Mihalcea, D.S. Baer, R.K. Hanson, Diode-laser absorption sensor for combustion emission measurements. *Meas. Sci. Technol.* **9**, 327–338 (1998)
  16. Nanosystems and Technologies GmbH, <http://www.nanoplus.com>
  17. A. Farooq, J.B. Jeffries, R.K. Hanson, CO<sub>2</sub> concentration and temperature sensor for combustion gases using diode-laser absorption near 2.7  $\mu\text{m}$ . *Appl. Phys. B* **90**, 619–628 (2008)
  18. A. Farooq, J.B. Jeffries, R.K. Hanson, Measurements of CO<sub>2</sub> concentration and temperature at high pressures using 1f-normalized wavelength modulation spectroscopy with second harmonic detection near 2.7  $\mu\text{m}$ . *Appl. Opt.* **48**, 2740–2753 (2009)
  19. A. Farooq, J.B. Jeffries, R.K. Hanson, Sensitive detection of temperature behind reflected shock waves using wavelength modulation spectroscopy of CO<sub>2</sub> near 2.7  $\mu\text{m}$ . *Appl. Phys. B* **96**, 161–173 (2009)
  20. R.M. Spearrin, C.S. Goldenstein, J.B. Jeffries, R.K. Hanson, Fiber-coupled 2.7  $\mu\text{m}$  laser absorption sensor for CO<sub>2</sub> in harsh combustion environments. *Meas. Sci. Technol.* **24**, 055107 (2013)
  21. M.E. Webber, S. Kim, S.T. Sanders, D.S. Baer, R.K. Hanson, Y. Ikeda, In situ combustion measurements of CO<sub>2</sub> by use of a distributed-feedback diode-laser sensor near 2.0  $\mu\text{m}$ . *Appl. Opt.* **40**, 821–828 (2001)
  22. R.M. Mihalcea, D.S. Baer, R.K. Hanson, Diode-laser absorption measurements of CO<sub>2</sub> near 2.0  $\mu\text{m}$  at elevated temperatures. *Appl. Opt.* **37**, 8341–8346 (1998)
  23. G.B. Rieker, J.B. Jeffries, R.K. Hanson, Measurements of high-pressure CO<sub>2</sub> absorption near 2.0  $\mu\text{m}$  and implications on tunable diode laser sensor design. *Appl. Phys. B* **94**, 51–63 (2009)
  24. L.S. Rothman, I.E. Gordon, Y. Babikov, A. Barbe, D. Chris Benner, P.F. Bernath, M. Birk, L. Bizzocchi, V. Boudon, L.R. Brown, A. Campargue, K. Chance, E.A. Cohen, L.H. Coudert, V.M. Devi, B.J. Drouin, A. Fayt, J.-M. Flaud, R.R. Gamache, J.J. Harrison, J.-M. Hartmann, C. Hill, J.T. Hodges, D. Jacquemart, A. Jolly, J. Lamouroux, R.J. Le Roy, G. Li, D.A. Long, O.M. Lyulin, C.J. Mackie, S.T. Massie, S. Mikhailenko, H.S.P. Müller, O.V. Naumenko, A.V. Nikitin, J. Orphal, V. Perevalov, A. Perrin, E.R. Polovtseva, C. Richard, M.A.H. Smith, E. Starikova, K. Sung, S. Tashkun, J. Tennyson, G.C. Toon, V.I. Tyuterev, G. Wagner, The HITRAN2012 molecular spectroscopic database. *J. Quant. Spectrosc. Radiat. Transf.* **130**, 4–50 (2013)
  25. L.S. Rothman, I.E. Gordon, R.J. Barber, H. Dothe, R.R. Gamache, A. Goldman, V.I. Perevalov, S.A. Tashkun, J. Tennyson, HITEMP, the high-temperature molecular spectroscopic database. *J. Quant. Spectrosc. Radiat. Transfer* **111**, 2139–2150 (2010)
  26. T.D. Cai, G.S. Wang, H. Jia, W.D. Chen, X.M. Gao, A sensor for measurements of temperature and water concentration using a single tunable diode laser near 1.4  $\mu\text{m}$ . *Sens. Actuators A* **152**(1), 5–12 (2009)
  27. H. Li, G.B. Rieker, X. Liu, J.B. Jeffries, R.K. Hanson, Extension of wavelength-modulation spectroscopy to large modulation depth for diode laser absorption measurements in high-pressure gases. *Appl. Opt.* **45**, 1052–1061 (2006)
  28. X. Zhou, X. Liu, J.B. Jeffries, R.K. Hanson, Development of a sensor for temperature and water concentration in combustion gases using a single tunable diode laser. *Meas. Sci. Technol.* **14**, 1459–1468 (2003)
  29. P. Kluczynski, O. Axner, Theoretical description based on Fourier analysis of wavelength-modulation spectrometry in terms of analytical and background signals. *Appl. Opt.* **38**, 5803–5815 (1999)
  30. S.R. Drayson, Rapid computation of the Voigt profile. *J. Quant. Spectrosc. Radiat. Transfer* **16**, 611–614 (1976)